Solar Phys (2016) 291:265–284
DOI 10.1007/s11207-015-0806-9

Relationships Among Geomagnetic Storms, Interplanetary Shocks, Magnetic Clouds, and Sunspot Number During 1995 – 2012

Chin-Chun Wu[1] · Ronald P. Lepping[2]

Received: 18 June 2015 / Accepted: 20 October 2015 / Published online: 24 November 2015

Abstract During 1995 – 2012, the *Wind* spacecraft has recorded 168 magnetic clouds (MCs), 197 magnetic cloud-like structures (MCLs), and 358 interplanetary (IP) shocks. Ninety-four MCs and 56 MCLs had upstream shock waves. The following features are found: i) The averages of the solar wind speed, interplanetary magnetic field (IMF), duration ($\langle \Delta t \rangle$), the minimum of $B_{\rm min}$, and intensity of the associated geomagnetic storm/activity ($\rm Dst_{min}$) for MCs with upstream shock waves ($\rm MC_{shock}$) are higher (or stronger) than those averages for the MCs without upstream shock waves ($\rm MC_{no\text{-}shock}$). ii) The average $\langle \Delta t \rangle$ of $\rm MC_{shock}$ events ($\approx$ 19.8 h) is 9 % longer than that for $\rm MC_{no\text{-}shock}$ events ($\approx$ 17.6 h). iii) For the $\rm MC_{shock}$ events, the average duration of the sheath ($\langle \Delta t_{\rm sheath} \rangle$) is 12.1 h. These findings could be very useful for space weather predictions, *i.e.* IP shocks driven by MCs are expected to arrive at *Wind* (or at 1 AU) about 12 h ahead of the front of the MCs on average. iv) The occurrence frequency of IP shocks is well associated with sunspot number (SSN). The average intensity of geomagnetic storms measured by $\langle \rm Dst_{min} \rangle$ for $\rm MC_{shock}$ and $\rm MC_{no\text{-}shock}$ events is -102 and -31 nT, respectively. The average values $\langle \rm Dst_{min} \rangle$ are -78, -70, and -35 nT for the 358 IP shocks, 168 MCs, and 197 MCLs, respectively. These results imply that IP shocks, when they occur with MCs/MCLs, must play an important role in the strength of geomagnetic storms. We speculate about the reason for this. Yearly occurrence frequencies of $\rm MC_{shock}$ and IP shocks are well correlated with solar activity (*e.g.*, SSN). Choosing the correct $\rm Dst_{min}$ estimating formula for predicting the intensity of MC-associated geomagnetic storms is crucial for space weather predictions.

Keywords Geomagnetic storms · Interplanetary shocks · Magnetic clouds · Solar activity · Solar cycle · Space weather

✉ C.-C. Wu
Chin-Chun.Wu@nrl.navy.mil

1 Naval Research Laboratory, Washington, DC 20375, USA

2 GSFC/NASA, Greenbelt, MD, USA

1. Introduction

A geomagnetic storm is one of the most important space weather events; it could damage operating space vehicles, interrupt radio communications, damage power plants, *etc*. The presence of a southward oriented interplanetary magnetic field (IMF) is one of the major solar wind features to affect the strength of geomagnetic activity. It is well known that a geomagnetic storm depends on the strength and duration of the solar wind IMF B_z component (in the Geocentric Solar Magnetospheric (GSM) coordinate system) and the speed of the associated impacting plasma parcel in which the field is imbedded (Tsurutani and Gonzalez, 1997), but likewise important is the size of the magnetosphere at the time of this interaction (*e.g.*, Shue *et al.*, 1998). The size of the magnetosphere is known to depend on the instantaneous solar wind dynamic (or ram) pressure: a strong ram pressure causes the magnetosphere to significantly decrease on the front-side (and elsewhere) and, in turn, result in a strong northern internal magnetic field at the front-side magnetopause. If a relatively strong increase in ram pressure occurs just before the interaction of an intense and long-lasting IMF B_z component, the expected magnetic merging at the magnetopause will be unusually strong because the magnetic field is intense on both sides of the front-side magnetopause for any fixed IP speed.

A geomagnetic storm can be caused by a southward IMF associated with an interplanetary (IP) shock wave (sheath), a magnetic cloud (MC), heliospheric current sheet sector boundary crossing, and combinations of these interplanetary structures (*e.g.*, Echer and Gonzalez, 2004). A strong geomagnetic storm can be produced by the interaction between an IP shock and an MC (*e.g.*, Wang *et al.*, 2003) or the interaction among multiple MC events (including upstream shock) (*e.g.*, Wang *et al.*, 2003). The largest geomagnetic storm of Solar Cycle 23, which occurred on 20 November 2003 (Dst dropped to −472 nT), was caused by the combination of a southward IMF behind the IP shock wave (a sheath region) and an MC itself (Gopalswamy *et al.*, 2005). Tsurutani and Gonzalez (1997) reviewed the interplanetary (IP) cause of magnetic storms. They discussed the various IP magnetic field configurations that can trigger geomagnetic storms, including magnetic clouds and various sheath field configurations (Figure 6).

An MC is defined as a region of high magnetic field strength, low proton temperature, low proton beta, and smoothly changing (rotating) magnetic field (*e.g.*, Burlaga *et al.*, 1981). Inside of an MC there typically is a long-lasting relatively strong southward IMF. Therefore, MCs are one of the most geoeffective IP structures typically causing $\mathrm{Dst}_{\mathrm{min}} \leq -30$ nT (*e.g.*, Wu and Lepping, 2002a, 2011, 2015). On average, most MC events ($\approx$90 % MCs) induce geomagnetic storms, and $\approx$39 % of MCs generate intense geomagnetic storms (*e.g.*, Wu, Lepping, and Gopalswamy, 2006; Wu and Lepping, 2015). Magnetic clouds interacting with the geomagnetosphere usually have all of the ingredients to produce strong geomagnetic storms because they mostly move fast and have strong and long-lasting southward B_z components. Immediately upstream of many MCs, either a driven shock wave exists, which increases the ram pressure well above the typical value of 2.2 nPa, or a pressure pulse heading toward becoming a shock wave beyond 1 AU. The MC upstream-driven shock wave or pressure pulse, when they occur, are expected to significantly increase the solar wind ram pressure (sometimes to values as high as 25 nPa or higher), which usually remains elevated during the passage of the sheath-interval, that is, between the shock and the MC front.

A magnetic cloud-like (MCL) structure is found (initially as a candidate MC) by an automatic identification scheme (Lepping, Wu, and Berdichevsky, 2005) that uses the same criteria as for an MC, but the MCL structure in this case is apparently not a simple force-free flux rope after further examination. That is, strictly speaking, an MCL structure cannot

be shown to be a flux rope by using the MC-fitting model developed by Lepping, Burlaga, and Jones (1990), although it qualitatively appears to be an MC according to the original definition of Burlaga *et al.* (1981) (see also Burlaga 1988, 1995). We consider this to be an operational definition of an MCL. This lack of accommodation by this MC model with regard to MCLs may be due to one or more of many possibilities. For example, the attempted model fitting may not properly converge (usually the main reason), or the estimated closest approach may show a value of close to, or greater than, 1.0, or the χ^2 of the fit may be excessively large, or the estimated asymmetry may be unacceptably large, *etc.*; the details of a scheme for assessing quality of an MC fitting using the Lepping, Burlaga, and Jones (1990) fitting scheme are given by Lepping *et al.* (2006).

A so-called sudden storm commencement (SSC) is usually caused by either an IP shock or a strong pressure pulse colliding with Earth's magnetosphere. An SSC might be followed by a geomagnetic storm, if the IMF is strong enough and remains southward for a long enough period of time, and if is fast enough. An IP shock or pressure pulse may be driven by an MC, a corotating interaction region (CIR), or other IP structures. Previous study shows that more than approximately half of the MCs observed by *Wind* have upstream shocks (Lepping *et al.*, 2002, 2015). The average intensity of $\mathrm{Dst_{min}}$ associated with IP shocks is $\langle \mathrm{Dst_{min}} \rangle = -74.6$ nT (Wu and Lepping, 2008). This does not mean that IP shocks directly cause geomagnetic storms. It may be that the $\mathrm{Dst_{min}}$ is indirectly related to the shock through the creation of a sheath – if B_z is southward in that sheath. A possible southward B_z field in the sheath probably is a condition itself for a geomagnetic storm, possibly in combination with the MC, causing a dual storm (or a two-step storm). The average storm intensity associated with MCs is -70 nT (*e.g.*, Wu and Lepping, 2015), which is relatively high, and it is believed that the very largest $\mathrm{Dst_{min}}$s are usually caused by MCs; an example is the storm of 13 – 14 March 1989, which had a $\mathrm{Dst_{min}} = -589$ nT, and was caused by an MC. All of this motivates us to statistically examine MCs and MCLs, along with their possible driven upstream shock waves, in their role as generators of geomagnetic storms.

The *Wind* spacecraft has collected solar wind *in situ* data for more than 20 years (1995 – mid-2015). The data set (1995 – 2012) used in this work provides a good opportunity for statistically studying the long-term effects of MCs/MCLs and IP shocks on geomagnetic storms, and in relation to the sunspot number (SSN). Data analysis and results are given in Section 2, and the summary is given in Section 3.

2. Data Analysis and Results

Five data sets were used in this study. The first data set, *Wind* solar wind plasma and magnetic field data, was obtain from the NASA (USA) *Wind* Solar Wind Experiment (SWE) and Magnetic Field Investigation (MFI) teams (http://cdaweb.gsfc.nasa.gov/pub/data/wind). The second data set, MCs for January 1995 to December 2009, is listed on the *Wind*/MFI web-site (http://lepmfi.gsfc.nasa.gov/mfi/mag_cloud_pub1.html), and the 2010 – 2012 MCs are listed in Lepping *et al.* (2012, 2015). MCLs can be found in Wu and Lepping (2015). The third data set, the geomagnetic activity index, Dst is obtained from both the National Geophysical data Center, Boulder, Colorado, USA and Kyoto University, Kyoto, Japan. The fourth data set, a list of *Wind* IP shocks, is obtained from Harvard–Smithsonian Center for Astrophysics Interplanetary Shock Database (https://www.cfa.harvard.edu/shocks/wi_data/). The fifth data set, solar activity or the SSN, was obtained from the National Geophysical data Center, Boulder, Colorado, USA.

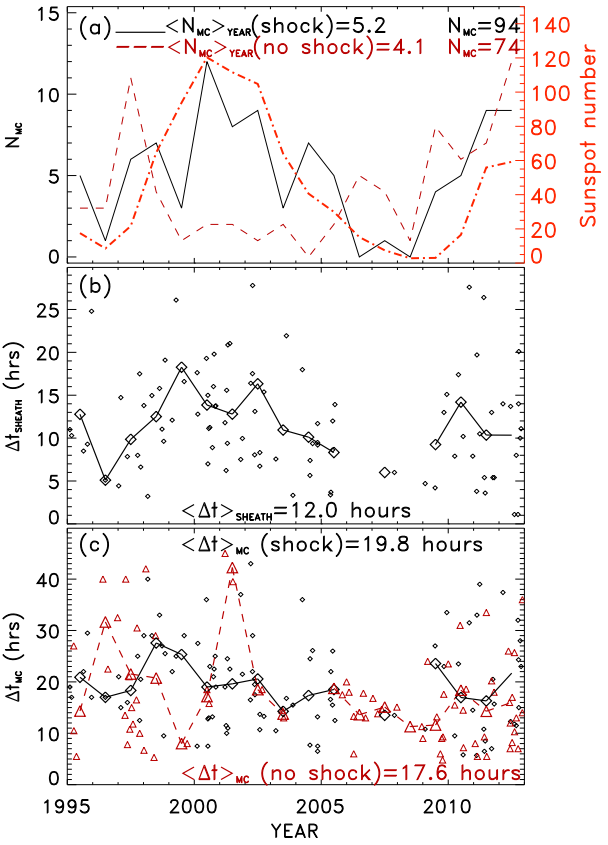

Figure 1 (a) The occurrence frequency of MC_{shock} and $MC_{no\text{-}shock}$ events, (b) duration of the sheath (Δt_{sheath}) for MC_{shock} (middle panel), and (c) duration of MCs for both MC_{shock} (red diamond, black solid diamond line is the yearly average) and $MC_{no\text{-}shock}$ (red dashed and triangles) events (bottom panel) during 1995 – 2012. The small black diamonds and red triangles represent Δt for the MC_{shock} events and for $MC_{no\text{-}shock}$ events, respectively. Black solid diamond and red dashed triangle lines represent yearly averages for MC_{shock} and $MC_{no\text{-}shock}$ events, respectively.

2.1. Occurrence Frequency of MCs with Upstream Shock Waves

We identified 168 MCs in *Wind in situ* solar wind and magnetic field data during 1995 – 2012 (*e.g.*, Lepping *et al.*, 2015). Viewing upstream (up to 30 h) of each of the 168 MCs, 94 MCs were seen to have upstream shock waves, and 74 MCs did not have upstream shock waves; we justify the reasonableness of the 30 h-limit on Δt_{sheath} below. This means that 56 % of the *Wind*-observed MCs had upstream shock waves when the full interval of 1995 – 2012 is considered, which is consistent with past findings using a smaller data set (Lepping *et al.*, 2002).

Figure 1a shows the time profile of MC_{shock} (as a black solid line) and $MC_{no\text{-}shock}$ (as a red dashed line) events for the yearly occurrence frequency N_{MC} and sunspot number (as an orange dot-dashed line). Figure 1b shows the duration of the sheaths (Δt_{sheath}), and Figure 1c shows the duration of the MCs (Δt_{MC}), during 1995 – 2012. We note that "sheath", as used above, means the region between the IP-driven shock and the front boundary of the MC. The black solid lines and red dashed lines represent yearly averaged values. The yearly occurrence rate of MC_{shock} and $MC_{no\text{-}shock}$ is 5.2 and 4.1, respectively. The average of Δt_{sheath} ($\langle \Delta t_{sheath} \rangle$) is 12.0 h (black diamond solid line), and $\sigma_{\Delta t}$ is 6.5 h, but values as low as 1.1 h and as high as $\approx$30 h have been observed. The average of Δt_{MC} for the MC_{shock} events ($\langle \Delta t_{MC} \rangle = 19.8$ h and $\sigma_{\Delta t} = 11.0$ h) is $\approx$11 % longer than that for the $MC_{no\text{-}shock}$ events ($\langle \Delta t_{MC} \rangle = 17.6$ h). We note that $[\langle \Delta t_{sheath} \rangle + 2 \times \sigma(\Delta t)]$ for MCs is (12.0+13.0) h = 25.0 h.

This means that our choice of 30 h for the limit of $\Delta t_{\rm sheath}$ values, when examining the data, further ensures that very few IP shocks are missed.

Figure 1a shows that the occurrence frequency of $\rm MC_{shock}$ is associated with solar activity. The correlation coefficient (CC) for SSN *vs.* $N_{\rm MC}$ (for shocks) is 0.7. For example, the peak of $N_{\rm MC}$ (for shocks) occurred in 2000, no $\rm MC_{shock}$ in 2006 and 2008, and only one $\rm MC_{shock}$ in 1996 and in 2007. In addition, $\langle \Delta t_{\rm sheath} \rangle$ is also associated with solar activity (see Figure 1b): i) $\langle \Delta t_{\rm sheath} \rangle$ is much longer in the solar active period, *e.g.*, $\langle \Delta t_{\rm sheath} \rangle > 10$ h in 2011 and during 1999 – 2002. ii) $\langle \Delta t_{\rm sheath} \rangle$ is shorter in the quiet period, *e.g.*, $\langle \Delta t_{\rm sheath} \rangle \approx 5$ h in 1996 and in 2008. In contrast (see Figure 1c), $\langle \Delta t_{\rm MC} \rangle$ is not well associated with solar activity.

2.2. Solar Wind Variation of MCs and Sheath Parameters

Figure 2 shows the averages of solar wind parameters in the sheath for the 94 $\rm MC_{shock}$ events. Over the long-term period (1995 – 2012), the average density $\langle N_{\rm p} \rangle$ is 15.8 $\rm cm^{-3}$, the velocity $\langle V \rangle$ is 513 $\rm km\,s^{-1}$, the magnetic field $\langle B \rangle$ is 13.2 nT, the thermal speed $\langle V_{\rm th} \rangle$ (or temperature) is 49.2 $\rm km\,s^{-1}$, the minimum $B_z \langle B_{z,\rm min} \rangle$ is -15.3 nT, and the associated geomagnetic storm intensity $\langle \rm Dst_{min} \rangle$ is -102 nT. We point out that $\langle V_{\rm th} \rangle$, $\langle V \rangle$, and $\langle B \rangle$ are higher in the solar active period than they are in the quiet period. For example, $\langle V_{\rm th} \rangle$ was 20 $\rm km\,s^{-1}$ in 1996, but was 80 $\rm km\,s^{-1}$ in 2003 (see Figure 2c).

Figure 3 shows the time profile of various solar wind parameters inside an MC for both $\rm MC_{shock}$ (black diamonds) and $\rm MC_{no\text{-}shock}$ (red triangles) events. Black solid diamond curves and red dashed triangle curves represent yearly averages for $\rm MC_{shock}$ and $\rm MC_{no\text{-}shock}$ events, respectively. The averages of the solar wind speed (V), magnitude of IMF ($B_{\rm MC}$), strength of $B_{z,\rm min}$, and the associated intensity of the geomagnetic activity ($\rm Dst_{min}$) for $\rm MC_{shock}$ events are higher or stronger than those for the $\rm MC_{no\text{-}shock}$ events. Comparing data for the sheaths (Figure 2) and for the MCs (Figure 3), we found the following, on average. i) The solar wind density in the sheath ($N_{\rm p,sheath}$) is about 90 % higher than inside the MCs. ii) The solar wind velocity in the sheath is 5 % faster than in the MC. iii) The solar wind temperature is higher in the sheath than in the MC by 98.4 % [$= (49.2 - 24.8)/24.8$]. Finally, iv) the magnitude of the magnetic field and strength of $B_{z,\rm min}$ are stronger for the MC than for the sheath.

2.3. Some Relationships Among MCs/MCLs, IP Shocks, Geomagnetic Activity, and SSN

Figure 3 shows an interesting result: the $\langle \rm Dst_{min} \rangle$ for $\rm MC_{shock}$ events (-102 nT) is ≈ 3.3 times stronger than for the $\rm MC_{no\text{-}shock}$ events ($\langle \rm Dst_{min} \rangle = -31$ nT). This is mainly due to the following two features: i) the difference in the strengths of the southward IMFs inside of the MCs (or in the sheath regions) for these two conditions, *viz.*, $\langle B_{z,\rm min} \rangle$ is -17.4 nT for $\rm MC_{shock}$, but is -6.0 nT for $\rm MC_{no\text{-}shock}$; and ii) the dynamic pressure operating on the magnetosphere for the shock cases: the increased strength of the Earth's field just inside the magnetopause due to the increased dynamic pressure of the impinging shock or sheath. For example, $\langle B_{z,\rm min} \rangle$ inside the MCs is -9.2, -12.8, and -6.0 nT for all MCs, $\rm MC_{shock}$, and $\rm MC_{no\text{-}shock}$ events, respectively (see the last column of Table 1). These findings should be useful for space weather prediction, *i.e.* MC-driven IP shocks typically arrive at *Wind* (or 1 AU) about 12 h ahead of the MCs. The arrival of an MC-driven IP shock could be used as a pre-cursor of the MC. Therefore, knowledge of such IP shocks could play an important role in estimating the timing and intensity of geomagnetic storms.

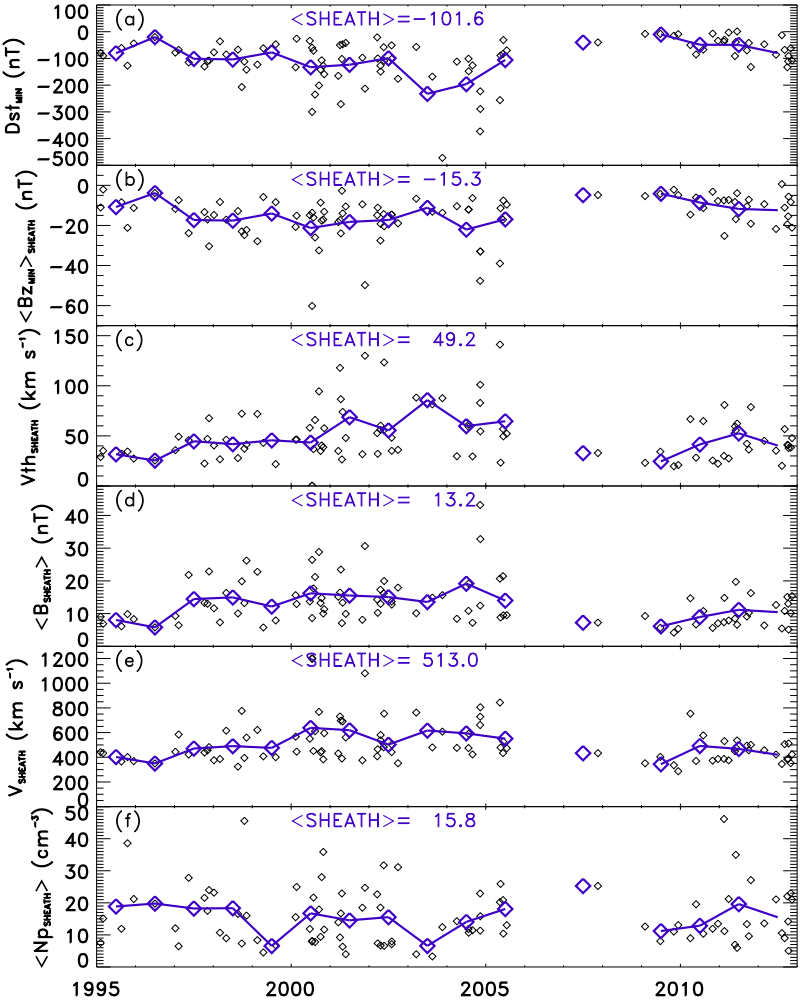

Figure 2 Averages of various solar wind parameters of the sheath for the 94 MC_{shock} events. Bottom to top: averages of density (N_p), velocity (V), magnetic field (B), thermal speed (V_{th}), minimum B_z ($B_{z,min}$), Δt_{sheath}, and associated geomagnetic activity (Dst_{min}).

IP shocks are not only important for MC-magnetosphere interactions, they are also important for MCL – magnetosphere interactions. For example, $\langle Dst_{min} \rangle$ are −35, −51, and −29 nT for all MCLs, MCL_{shock}, and $MCL_{no\text{-}shock}$ events, respectively (see Table 1, last column); these are significant values, although they are expected to be lower (in absolute value) than those for the MC events, as shown in the upper part of Table 1. $\langle Dst_{min} \rangle$ for the MCL_{shock} events is 1.8 times stronger than that for the $MCL_{no\text{-}shock}$ events. Again, $B_{z,min}$ is one of the major factors that affects the strength of Dst_{min} for the events associated with MCLs. Solar wind density, temperature (thermal speed, V_{th}), speed, and magnetic field for MCL_{shock} events are all higher for the shock-related MCs than for $MCL_{no\text{-}shock}$ events. Out of 197 MCLs, only 56 have upstream shock waves. Only 28 % of MCL events are MCL_{shock} types. The IP shock occurrence rate for MCs is twice that for the MCLs.

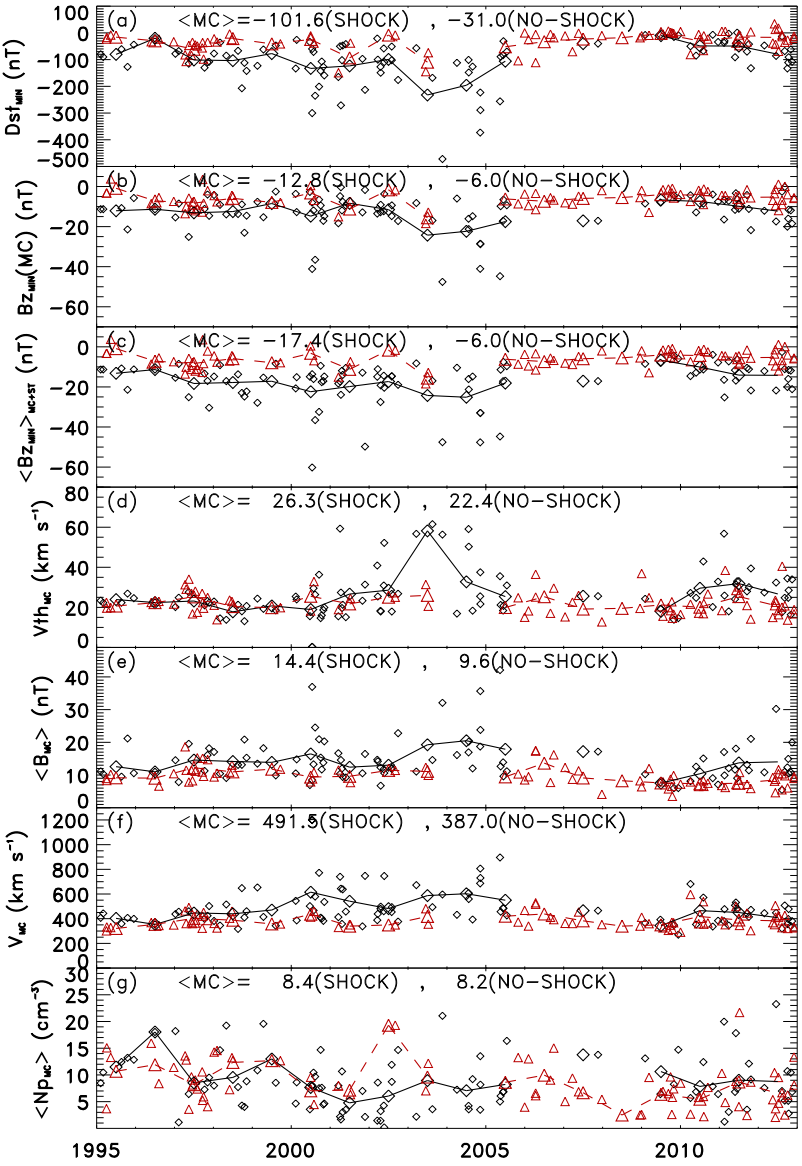

Figure 3 Time profile of various solar wind parameters inside MCs for both MC_{shock} and $MC_{no\text{-}shock}$ events. Small black diamonds and small red triangles represent events for MC_{shock} and $MC_{no\text{-}shock}$, respectively. Black diamond curves and red triangle curves represent yearly averages for MC_{shock} and $MC_{no\text{-}shock}$, respectively.

As stated above, IP shocks can play an important role in affecting the strength of geomagnetic storms (*e.g.*, Wu and Lepping, 2008). An SSC is an indication of an IP shock arrival at Earth, just before the storm. Table 1 confirms (for MC cases) that IP shocks play an important role in affecting geomagnetic activity. For MCLs, $\langle Dst_{min} \rangle$ for MCL_{shock} events is 1.8 times stronger than that for the $MCL_{no\text{-}shock}$ events. These results are consistent with previ-

Table 1 Averages of solar wind parameters of MCs and MCLs observed by *Wind* during 1995 – 2012.

	N_T[a]	Δt[b] [h]	N_p [cm^{-3}]	V [$km\,s^{-1}$]	B [nT]	V_{th} [$km\,s^{-1}$]	$B_{z,min}$ [nT]	$VB_{s,max}$	Dst_{min} [nT]
MC	168	18.8	8.2	440	12.3	24.8	−9.8	5.1	−70
MC_{shock}[c]	94	19.8	8.2	482	14.4	26.8	−12.8	7.1	−102
MC_{sheath}[d]		12.1	7.2	502	13.4	49.2	−12.1	5.8	
$MC_{no\text{-}shock}$[e]	74	17.6	8.2	387	9.6	22.4	−6.0	2.5	−31
MCL	197	15.7	6.3	404	9.5	25.5	−5.6	2.3	−35
MCL_{shock}[c]	56	17.8	5.9	444	10.5	26.2	−6.2	2.9	−51
MCL_{sheath}[d]		15.3	12.5	469	11.4	40.9	−10.1	4.3	
$MCL_{no\text{-}shock}$[e]	141	14.9	6.4	388	9.2	25.2	−5.4	2.1	−29
Shock	357								−78

[a]Total number of MC/MCL events.

[b]Duration of MC/MCL; $\langle \Delta t_{MC} \rangle_{sheath} = 12.1$ h, $\langle \Delta t_{MCL} \rangle_{sheath} = 15.3$ h.

[c]MC/MCL events that have upstream shock waves.

[d]Sheath region, *i.e.* the region between the IP shock and the front boundary of the MC/MCL.

[e]MC/MCL events that have no upstream shock waves.

ous studies that showed that MCs are among the most important interplanetary structures in causing strong geomagnetic storms (*e.g.*, Wu and Lepping 2002a, 2002b, 2005, 2007; Wu, Lepping, and Gopalswamy, 2003); on average, the geomagnetic activity is more strongly affected by MCs than by MCLs or IP shocks alone (*e.g.*, Wu and Lepping, 2008).

It is also well known that most IP shocks recorded at 1 AU are driven by solar ejecta (*e.g.*, MCs, IP coronal mass ejections). The *Wind* spacecraft has recorded 358 IP shocks during 1995 – 2012 (see the blue dot-dashed line in Figure 4 for the yearly occurrence rate, N_{shock}). The yearly occurrence frequency of IP shocks is $\langle N_{shock} \rangle_{year} = 19.8$. The Dst index was checked two days after an IP shock arrived at L1 during 1995 – 2012. The average of Dst_{min} for these 358 IP shocks is $\langle Dst_{min} \rangle_{shock} = -78$ nT. The combined effects of both the southward IMF in the sheath and in the MC could cause a strong or even a severe geomagnetic storm, which is the so-called two-step storm (*e.g.*, Kamide *et al.*, 1998; Tsurutani *et al.*, 1997; Wu and Lepping, 2002a). The MC_{shock} events are usually associated with the strongest geomagnetic storms, *i.e.*, $\langle Dst_{min} \rangle = -102$ nT (see Table 1).

The CCs for SSN *vs.* occurrence rates for MCs, MC_{shock}, and $MC_{no\text{-}shock}$ events are 0.27, 0.70, and −0.29, respectively (see the designations in Figure 4a). The CCs for SSN *vs.* occurrence rates for MCLs, MCL_{shock}, and $MCL_{no\text{-}shock}$ events are 0.85, 0.87, and 0.79, respectively (see the designations in Figure 4b). The CCs for SSN *vs.* N_{MC} for both MC_{shock} and MCL_{shock} are greater than 0.70. Therefore, $\langle N_{shock} \rangle$ is reasonably well associated with SSN. This result is consistent with our previous study (Wu and Lepping, 2008): the occurrence frequency of sudden storm commencements (N_{SSC}) is reasonably well correlated with SSN, where CC for N_{SSC} *vs.* SSN is 0.77. We note that from mid-2003, *Wind* moved behind the Earth's bow shock and remained there for approximately nine months. Without using data for 2003 and 2004, the CC for SSN *vs.* occurrence rate for MC_{shock} increases to 0.79. Figure 4 shows that there is a well-correlated trend between IP shocks (dash-dot-dotted line) and SSN (dash-dotted lines), where the CC is 0.79 between them.

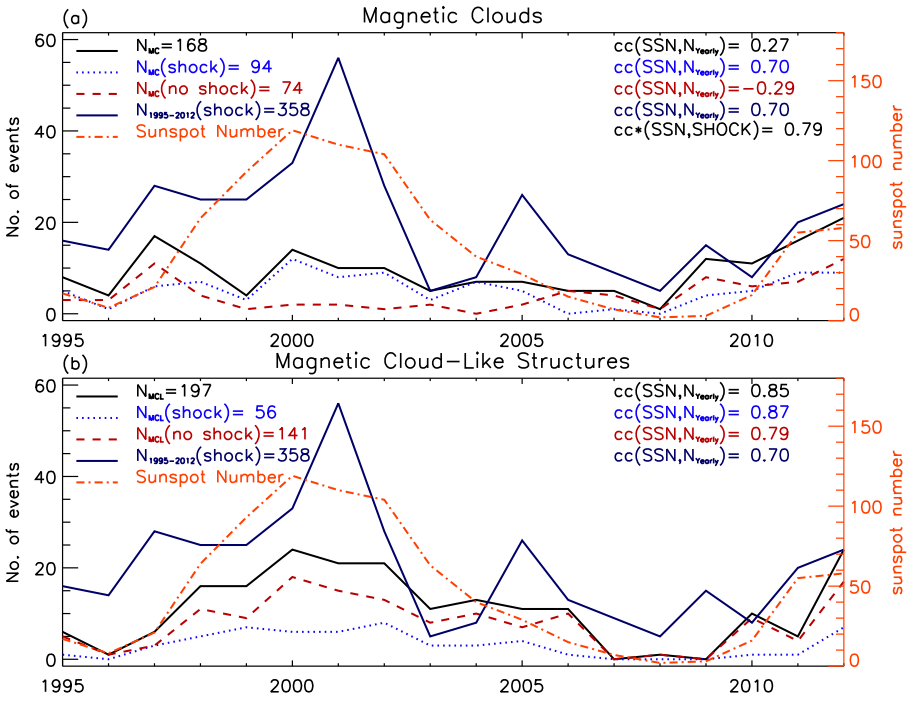

Figure 4 (a) Yearly occurrence frequency of MCs (black solid line), MCs with upstream shock wave (blue dotted line), MCs without upstream shock (red dashed line), and IP shock waves (dark blue dash-dot-dot-dotted line), and sunspot numbers (orange dot-dashed line). (b) Yearly occurrence frequency of MCLs (black solid line), MCLs with upstream shock wave (blue dotted line), MCLs without upstream shock (red dashed line), IP shock waves (dark blue dash-dot-dot-dotted line), and sunspot numbers (orange dot-dashed line). Total numbers (1995 – 2012) of MCs/MCLs are marked in the top left corner. The correlation coefficient (CC) between yearly sunspot number (SSN) and yearly occurrence frequency of MCs/MCLs are marked in the top-right corner.

This study shows that 56 % of the total observed MCs have upstream shock waves when the full interval of 1995 – 2012 is considered, but only 28 % (or 56 out of 197) of MCLs have shock waves over the same period (see Table 1). The values of $\langle \mathrm{Dst_{min}} \rangle$ for MCLs, $\mathrm{MCL_{shock}}$, and $\mathrm{MCL_{no\text{-}shock}}$ events are −35, −51, and −29 nT, respectively. For MC events, the yearly occurrence frequency of MC-driven shocks is associated with sunspots (CC = 0.70). The duration of the sheath ($\Delta t_{\mathrm{sheath}}$) is also correlated with SSN: on average, $\Delta t_{\mathrm{sheath}}$ in the solar active period was longer than that in the quiet solar period (see Figure 1a). The yearly occurrence rate of $\mathrm{MC_{shock}}$ and $\mathrm{MC_{no\text{-}shock}}$ is 5.2 and 4.1, respectively.

For MCs events, the IP $B_{z,\mathrm{min}}$ is a good indicator for estimating $\mathrm{Dst_{min}}$ because $\mathrm{Dst_{min}}$ is well correlated with $B_{z,\mathrm{min}}$ (*e.g.*, Wu and Lepping 2008, 2011, 2015). The intensity of a geomagnetic storm ($\mathrm{Dst_{min}}$) is predictable if $B_{z,\mathrm{min}}$ is known in advance, provided V_{SW} is known. However, the correlation coefficient (CC) of $\mathrm{Dst_{min}}$ *vs.* $B_{z,\mathrm{min}}$ varies somewhat with different data types, but the spread is small. For example, the CCs are 0.75, 0.85, 0.69, 0.82, 0.68, and 0.68 for $B_{z,\mathrm{min}}$ obtained in the (a) MC, (b) MC or sheath, (c) $\mathrm{MC_{shock}}$, (d) $\mathrm{MC_{shock}}$ or sheath, (e) sheath, (f) $\mathrm{MC_{no\text{-}shock}}$, respectively (see column 5 in Table 2). The CC is higher for $\mathrm{MC_{shock}}$ events than that for $\mathrm{MC_{no\text{-}shock}}$ events.

Table 2 Estimating $\mathrm{Dst_{min}}$ formulae obtained from a linear fit of $B_{z,\mathrm{min}}$.

	Event	$\mathrm{Dst_{min}}$ formula[a]	$\langle \mathrm{Dst_{min}} \rangle$[b]	CC[c]	Source of $B_{z,\mathrm{min}}$
(a)	168 MCs	$\mathrm{Dst_{min}} = -3.30 + 6.82 \times B_{z,\mathrm{min}}$	−70	0.75	MC
(b)	168 MCs	$\mathrm{Dst_{min}} = 8.04 + 6.34 \times B_{z,\mathrm{min}}$	−70	0.85	Sheath of MC
(c)	94 $\mathrm{MC_{shock}}$	$\mathrm{Dst_{min}} = -22.89 + 6.12 \times B_{z,\mathrm{min}}$	−102	0.69	MC
(d)	94 $\mathrm{MC_{shock}}$	$\mathrm{Dst_{min}} = 11.01 + 6.47 \times B_{z,\mathrm{min}}$	−102	0.82	Sheath or MC
(e)	94 $\mathrm{MC_{shock}}$	$\mathrm{Dst_{min}} = -21.18 + 5.26 \times B_{z,\mathrm{min}}$	−102	0.68	Sheath
(f)	74 $\mathrm{MC_{no\text{-}shock}}$	$\mathrm{Dst_{min}} = 4.18 + 5.83 \times B_{z,\mathrm{min}}$	−30	0.68	MC

[a]Linear-fitted function for $\mathrm{Dst_{min}}$.

[b]Averaged $\mathrm{Dst_{min}}$.

[c]Pearson correlation coefficient for $\mathrm{Dst_{min}}$ *vs.* $B_{z,\mathrm{min}}$.

2.4. Effect of an IP Shock on the Intensity of a Geomagnetic Storm

An upstream shock wave of an $\mathrm{MC_{shock}}$ event typically arrives at Earth about 12 h ahead of the front boundary of the MC. An IP shock may be used as a precursor of a geomagnetic storm occasionally because 56 % of the MCs have upstream shock waves. Table 2 shows that $\mathrm{MC_{shock}}$ events generally associated with severe geomagnetic storms since $\langle \mathrm{Dst_{min}} \rangle$ is −102 nT for $\mathrm{MC_{shock}}$ events.

The value of $\langle \mathrm{Dst_{min}} \rangle$ for the $\mathrm{MC_{no\text{-}shock}}$ events is −31 nT. This means that most $\mathrm{MC_{no\text{-}shock}}$ events are not associated with strong geomagnetic storms, although many are, if $|B_{z,\mathrm{min}}|$ and V_{SW} are large, of course. This value is close to the value for MCLs ($\langle \mathrm{Dst_{min}} \rangle_{\mathrm{MCLs}} = -35$ nT). Therefore, an IP shock may be a main contributor to the strength of a geomagnetic storm, even if indirect. About 90 % of the MCs are associated with geomagnetic storms ($\mathrm{Dst_{min}} < -30$ nT). IP shocks play an important role in geomagnetic activity because $\langle \mathrm{Dst_{min}} \rangle$ for $\mathrm{MC_{shock}}$ is 3.25 times stronger than for $\mathrm{MC_{no\text{-}shock}}$ events (see the top panel of Figure 3). But again this does not mean that an IP shock alone can cause a geomagnetic storm.

2.5. Formulae for Estimating $\mathrm{Dst_{min}}$

Figure 5 shows a distribution of geomagnetic $\mathrm{Dst_{min}}$ and IP $B_{z,\mathrm{min}}$ for 168 MCs (Figures 5a and 5b), 94 $\mathrm{MC_{shock}}$ (Figures 5c, 5d, and 5e), and 74 $\mathrm{MC_{no\text{-}shock}}$ (Figure 4f) during 1995 – 2012. The CCs for $\mathrm{Dst_{min}}$ *vs.* $B_{z,\mathrm{min}}$ are marked in the third line in the top-left corner of each panel. $B_{z,\mathrm{min}}$ is obtained from the inside of the MCs (in Figures 5a, 5c, and 5f), the sheath region (for Figure 5e), and either the sheath or the MC (Figures 5b and 5d). The red straight lines are the linear fitting functions for the estimates of $\mathrm{Dst_{min}}$ *vs.* $B_{z,\mathrm{min}}$. The actual fitted function for the $\mathrm{Dst_{min}}$ *vs.* $B_{z,\mathrm{min}}$ linear estimation is shown in the bottom of each panel, and the CC for $\mathrm{Dst_{min}}$ *vs.* $B_{z,\mathrm{min}}$ is denoted below the fitting function. This detailed information is also listed in Table 2. The largest two CCs (= 0.85 and 0.82) are obtained from either the sheath or the MC for the 168 MCs and 94 $\mathrm{MC_{shock}}$ events because $\mathrm{Dst_{min}}$ would occur in the sheath region or inside the MC. This shows that $B_{z,\mathrm{min}}$ statistically plays a major role in affecting the intensity of geomagnetic storms, as expected. It is crucial to use the correct estimator of $B_{z,\mathrm{min}}$ for predicting the storm intensity (*i.e.* $\mathrm{Dst_{min}}$).

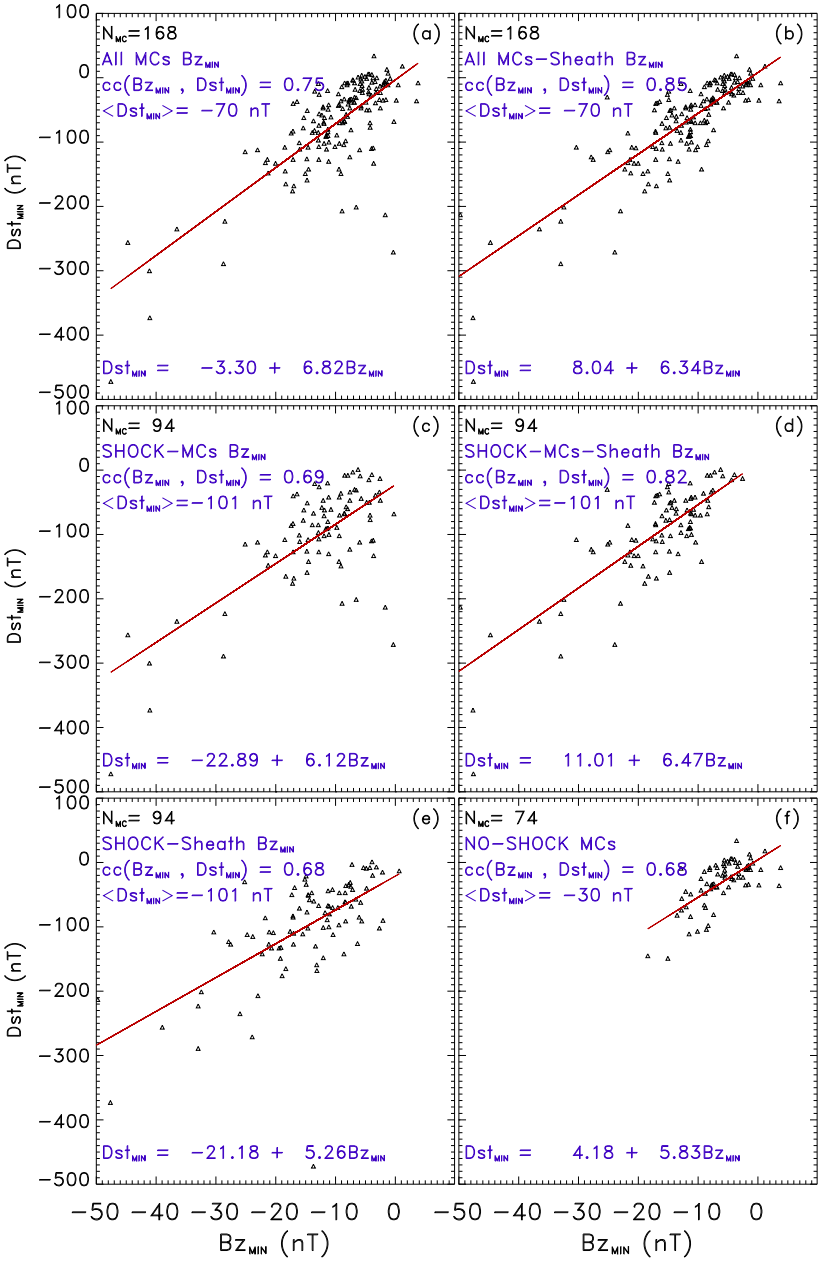

Figure 5 Distribution of geomagnetic storm intensity ($\mathrm{Dst_{min}}$) and minimum B_z ($B_{z,\mathrm{min}}$) for all MCs (panels a, b), MCs with upstream shock waves (panels c, d, e), and MCs without upstream shock (panel f) during 1995 – 2012. $\mathrm{Dst_{min}}$ linear fitting function and the correlation coefficients (CCs) are denoted at the top (the third line) and bottom of each panel, respectively. The averages of $\langle N_{\mathrm{MC}} \rangle$ and $\langle \mathrm{Dst_{min}} \rangle$ are denoted at the first and fourth lines at the top of each panel in respective order.

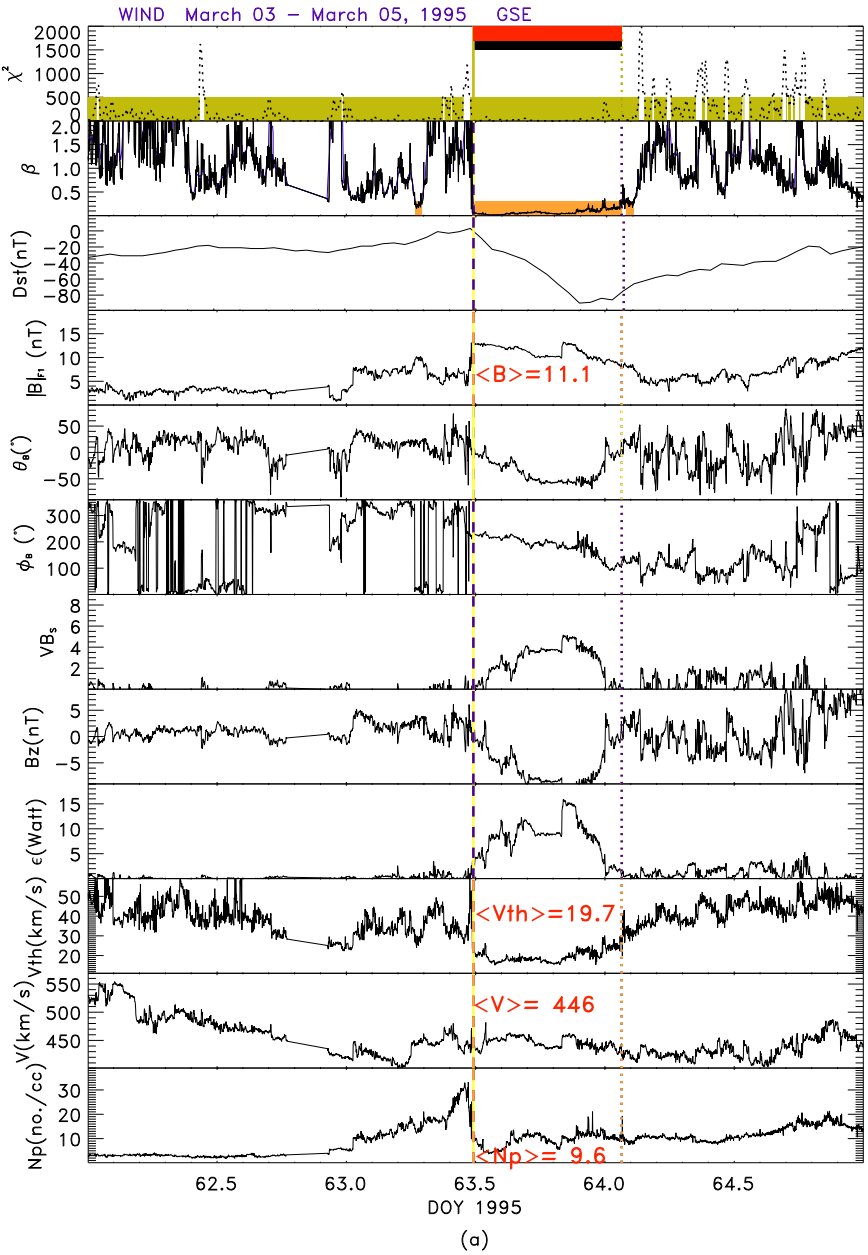

Figure 6 Examples of two MCs that were observed on 4 March 1995 (a) and on 17 September 2011 (b). From top to bottom: χ^2 of quadratic fit to latitude of the field (θ_B), running average of proton plasma beta (β) and dotted curve representing its running average, Dst, magnetic field (B) in terms of magnitude, latitude (θ_B) and longitude (ϕ_B) in GSE coordinates, induced electric field (VB_s), B_z of the field in GSE, ε (see Akasofu, 1981), proton plasma thermal speed (V_{th}), bulk speed (V), and number density (N_p). The red horizontal bar in the top panel represents the scheme identification of the extent of this MC candidate (Lepping, Wu, and Berdichevsky, 2005). The vertical yellow dashed line and blue dotted line represent front and rear boundaries identified by the MC automatic identifying model. The averages of N_p, V, V_{th}, and B for MC/MCL are provided in red in each panel.

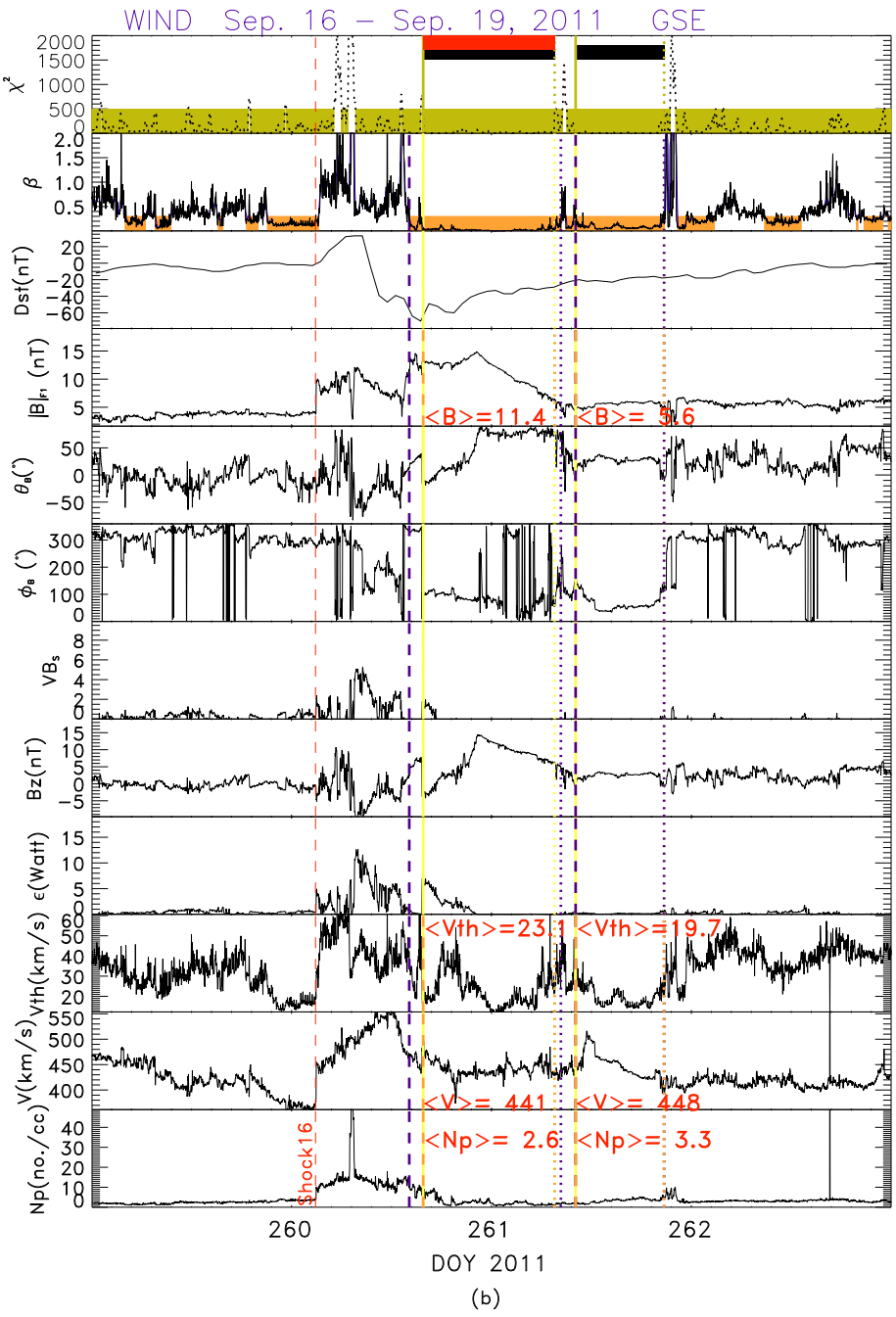

Figure 6 (*Continued.*)

Table 3 Estimated Dst_{min} for the geomagnetic storm caused by an MC event that occurred on 4 March 1995.

	Event	Dst_{min} formula[a]	$\langle B_{z,min}\rangle$[b] MC	$\langle Dst_{min}\rangle$[c] Pred.	Source of $B_{z,min}$	Error [%]
(a)	168 MCs	$Dst_{min} = -3.30 + 6.82 \times B_{z,min}$	−10	−71.5	MC	20.6
(b)	168 MCs	$Dst_{min} = 8.04 + 6.34 \times B_{z,min}$	−10	−55.36	Sheath of MC	38.5
(c)	94 MC_{shock}	$Dst_{min} = -22.89 + 6.12 \times B_{z,min}$	−10	−84.09	MC	7.6
(d)	94 MC_{shock}	$Dst_{min} = 11.01 + 6.47 \times B_{z,min}$	−10	−53.68	Sheath or MC	40.4
(e)	94 MC_{shock}	$Dst_{min} = -21.18 + 5.26 \times B_{z,min}$	−10	−73.78	Sheath	18.0
(f)	74 $MC_{no\text{-}shock}$	$Dst_{min} = 4.18 + 5.83 \times B_{z,min}$	−10	−54.12	MC	39.9

[a]Linear-fitted function for Dst_{min}.

[b]Averaged $B_{z,min}$.

[c]Predicted Dst_{min}.

Table 4 Estimating Dst_{min} by using $B_{z,min}$ for an MC event on 18 September 2011.

	Event	Dst_{min} formula[a]	$\langle B_{z,min}\rangle$[b] MC	$\langle Dst_{min}\rangle$[c] Pred.	Source of $B_{z,min}$	Error [%]
(a)	168 MCs	$Dst_{min} = -3.30 + 6.82 \times B_{z,min}$	−5	−37.4	MC	46.5
(b)	168 MCs	$Dst_{min} = 8.04 + 6.34 \times B_{z,min}$	−10	−55.36	Sheath of MC	20.9
(c)	94 MC_{shock}	$Dst_{min} = -22.89 + 6.12 \times B_{z,min}$	−5	−53.49	MC	23.6
(d)	94 MC_{shock}	$Dst_{min} = 11.01 + 6.47 \times B_{z,min}$	−10	−53.69	Sheath or MC	23.3
(e)	94 MC_{shock}	$Dst_{min} = -21.18 + 5.26 \times B_{z,min}$	−10	−73.78	Sheath	5.4
(f)	74 $MC_{no\text{-}shock}$	$Dst_{min} = 4.18 + 5.83 \times B_{z,min}$	−5	−24.97	MC	64.3

[a]Linear-fitted function for Dst_{min}.

[b]Averaged $B_{z,min}$.

[c]Predicted Dst_{min}.

2.6. Evaluating the Formulae for Estimating Dst_{min}

Figure 6a shows an example of an MC that induced a severe geomagnetic storm. The value of Dst_{min} is −90 nT, which is caused by a $B_{z,min}$ of −10 nT in the MC. Figure 1a clearly shows that the MC is an isolated solar disturbance (or event) that did not interact with any other kind of interplanetary structure [*e.g.*, heliosphere current sheet (HCS), co-rotating interaction region (CIR), another MC, or interplanetary coronal mass ejection (ICME)]. The direction of the IMF was changing smoothly from the front boundary to the end boundary of the MC, and an obvious driven shock was about 0.5 day ahead of the MC front boundary.

With the estimating Dst_{min} formulae (a) through (f) in Table 2, the estimated Dst_{min} are −71.5, −55.36, −84.09, −53.68, −73.78, and −54.12 nT, and the errors of prediction ($|Dst_{prediction} - Dst_{observation}|/|Dst_{observation}| \times 100$ %) are 20.6 %, 38.5 %, 7.6 %, 40.4 %, 18.0 %, and 39.9 %, respectively (see also the details in Table 3). Formula (c) gives the best estimate; it is based on the events that have upstream shock waves, and where $B_{z,min}$ inside the MC was used.

Figure 6b shows another example: an MC (that occurred on 18 September 2011) has an upstream shock (on 17 September) that induced a sheath geomagnetic storm

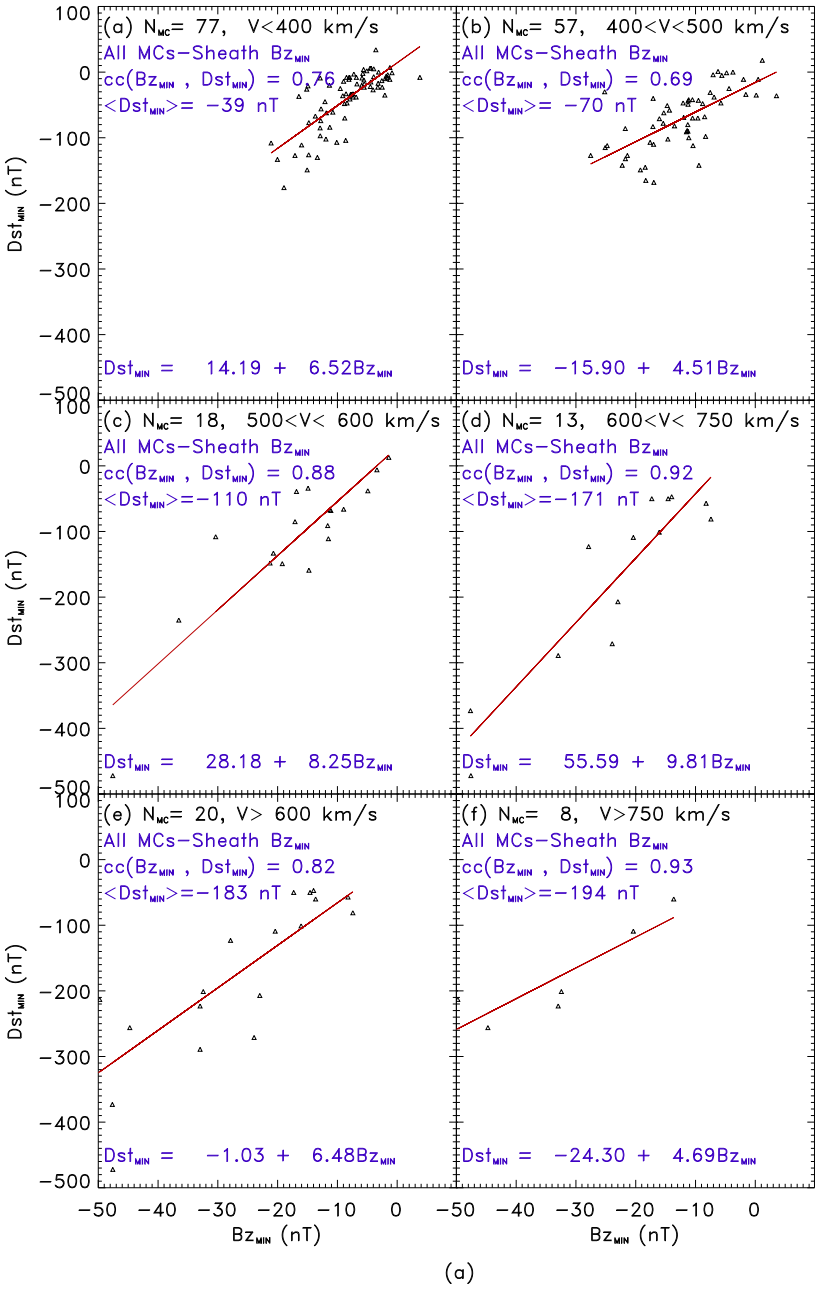

Figure 7 Distribution of geomagnetic storm intensity ($\mathrm{Dst_{min}}$) and minimum B_z ($B_{z,\mathrm{min}}$) for all MCs (A, top panel) and for MCs with upstream shock waves (B, bottom panel) during 1995 – 2012. $\mathrm{Dst_{min}}$ linear fitting function and the correlation coefficients (CCs) are denoted at the top (the third line) and bottom of each panel, respectively. The averages of $\langle N_{\mathrm{MC}} \rangle$ and $\langle \mathrm{Dst_{min}} \rangle$ are denoted at the first and fourth lines at the top of each panel in respective order.

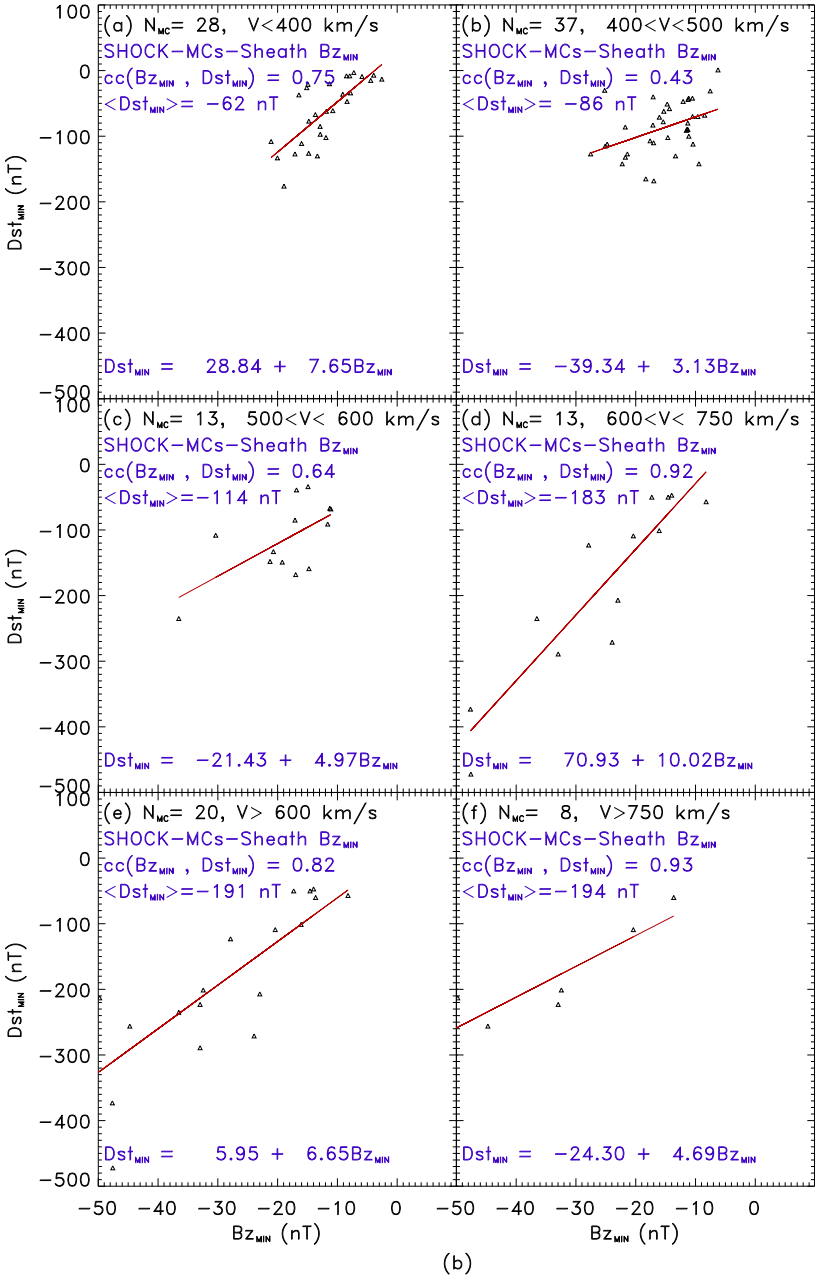

Figure 7 (*Continued.*)

($\mathrm{Dst_{min}} = -70$ nT). For this event, the $B_{z,\mathrm{min}}$ were -10 and -5 nT in the sheath and MC, respectively. Using the estimated $\mathrm{Dst_{min}}$ formulae (a), (b), (c), (d), (e), and (f) for the MC on 17 September 2011, the estimated $\mathrm{Dst_{min}}$ are -37.4, -55.36, -53.49, -53.69, -73.78, and -24.97 nT, and the errors of prediction are 46.5 %, 20.9 %, 23.6 %, 23.3 %, 5.4 %,

Table 5 Correlation coefficients between Dst_{min} and $B_{z,min}$ for various $\langle V_{MC} \rangle$ ranges.

Range of V [km s^{-1}]	All 168 MCs				94 MC driven shock events				
	# MCs	$\langle Dst_{min} \rangle$ [nT]	CC $B_{z,min}$ (MC)	CC $B_{z,min}$ (MC or Sheath)	# MCs	$\langle Dst_{min} \rangle$ (nT)	CC $B_{z,min}$ (MC)	CC $B_{z,min}$ (MC or Sheath)	CC $B_{z,min}$ (Sheath)
$V < 400$[a]	77[b]	−39[c]	0.73[d]	0.76[e]	28[f]	−62[g]	0.68[h]	0.75[i]	0.64[j]
$400 < V < 500$	56	−70	0.65	0.69	36	−85	0.45	0.45	0.46
$500 < V < 600$	17	−108	0.92	0.88	12	−109	0.81	0.69	0.41
$600 < V < 750$	12	−146	0.70	0.88	12	−179	0.82	0.92	0.52
$V > 750$	6	−208	0.66	0.91	6	−208	0.66	0.91	0.88
All events	168	−70	0.75	0.85	94	−102	0.69	0.82	0.68

[a]Range of the average MC speed.

[b]Number of events with a speed in this range.

[c]Average of the storm intensity for events with a velocity in this range.

[d]Correlation coefficients (CCs) of Dst_{min} versus $B_{z,min}$ in the MC.

[e]CCs of Dst_{min} versus $B_{z,min}$ obtained in the MC or in the sheath region.

[f]Number of MCs with upstream shock.

[g]Average of storm intensity for events with a velocity in this range.

[h]CCs of Dst_{min} versus $B_{z,min}$ obtained in the MC.

[i]CCs of Dst_{min} versus $B_{z,min}$ obtained in the MC or in the sheath region.

[j]CCs of Dst_{min} versus $B_{z,min}$ obtained in the sheath region.

and 64.3 %, respectively. Details can be found in Table 4. Formula (e) gave the best estimated Dst_{min}. Formula (e) was based on the events that had upstream shock waves and on using the sheath $B_{z,min}$ to obtain Dst_{min} in this case.

Dst_{min} *vs.* $B_{z,min}$ has a higher correlation for the MCs associated with higher speed than those with lower speed (*e.g.*, Wu and Lepping, 2002b). To understand the effects of solar wind velocity on geomagnetic storms, we cataloged MC events into different ranges of velocity. Figure 7 shows the relations between storm intensity (Dst_{min}) for various solar wind parameters for various $\langle V_{MC} \rangle$ ranges (correlation coefficients are also calculated and given in each panel). The distribution of the geomagnetic storm intensity (Dst_{min}) and minimum B_z ($B_{z,min}$) for all MCs is (left panel: A) and for MCs with upstream shock waves (right panel: B) during 1995 – 2012. Dst_{min} linear fitting function and the associated CCs are denoted at the top (the third line) and bottom of each panel, respectively. The averages of $\langle N_{MC} \rangle$ and $\langle Dst_{min} \rangle$ are denoted in the first and fourth lines at the top of each panel in respective order.

Tables 5 and 8 show the CCs between Dst_{min} and $B_{z,min}$ for various $\langle V_{MC} \rangle$ ranges. Figure 7 and Tables 5, 6, 7, 8 clearly show that the higher speed of MCs is associated with stronger geomagnetic storms (see the second column of Tables 5 – 8). Tables 5 – 8 also show that all MC events with speeds higher than 600 km s^{-1} have driven an IP shock. The CCs for Dst_{min} *vs.* $B_{z,min}$ (in MC or sheath) are higher for events with higher speeds. For events with speeds higher than 600 km s^{-1}, the CCs are higher than 0.8. This means that its Dst_{min} estimating function is reliable for performing space weather prediction.

Table 6 Estimating $\mathrm{Dst_{min}}$ formulae obtained from linear fit of $B_{z,\mathrm{min}}$ for various $\langle V_{\mathrm{MC}}\rangle$ ranges for 168 MCs observed during 1995 – 2012.

Range of V [km s^{-1}]	$\langle \mathrm{Dst_{min}}\rangle$ [nT]	Estimating Dst formula using $B_{z,\mathrm{min}}$ in MC	Estimating Dst formula using $B_{z,\mathrm{min}}$ in MC or sheath
$V < 400$[a]	−39[b]	$\mathrm{Dst_{min}} = 12.12 + 6.55B_{z,\mathrm{min}}$	$\mathrm{Dst_{min}} = 14.19 + 6.52B_{z,\mathrm{min}}$
$400 < V < 500$	−70	$\mathrm{Dst_{min}} = -21.08 + 4.82B_{z,\mathrm{min}}$	$\mathrm{Dst_{min}} = -16.14 + 4.50B_{z,\mathrm{min}}$
$500 < V < 600$	−108	$\mathrm{Dst_{min}} = -9.31 + 9.08B_{z,\mathrm{min}}$	$\mathrm{Dst_{min}} = 28.94 + 8.23B_{z,\mathrm{min}}$
$600 < V < 750$	−146	$\mathrm{Dst_{min}} = -70.76 + 6.55B_{z,\mathrm{min}}$	$\mathrm{Dst_{min}} = 36.18 + 8.65B_{z,\mathrm{min}}$
$V > 750$	−208	$\mathrm{Dst_{min}} = -147.07 + 2.84B_{z,\mathrm{min}}$	$\mathrm{Dst_{min}} = -32.14 + 4.54B_{z,\mathrm{min}}$

[a]Range of averaged speed inside of the MC.

[b]Average of storm intensity.

Table 7 Estimating $\mathrm{Dst_{min}}$ formulae obtained from linear fit of $B_{z,\mathrm{min}}$ for various $\langle V_{\mathrm{MC}}\rangle$ ranges for 94 MC driven shock events observed during 1995 – 2012.

Range of V [km s^{-1}]	Estimating Dst formula using $B_{z,\mathrm{min}}$ in MC[b]	Estimating Dst formula using $B_{z,\mathrm{min}}$ obtained in MC or Sheath[b]	Estimating Dst formula using $B_{z,\mathrm{min}}$ obtained in sheath[b]
$V < 400$[a]	$\mathrm{Dst_{min}} = 12.28 + 6.82B_{z,\mathrm{min}}$	$\mathrm{Dst_{min}} = 28.84 + 7.65B_{z,\mathrm{min}}$	$-10.83 + 5.42B_{z,\mathrm{min}}$
$400 < V < 500$	$\mathrm{Dst_{min}} = -43.37 + 3.37B_{z,\mathrm{min}}$	$\mathrm{Dst_{min}} = -36.69 + 3.21B_{z,\mathrm{min}}$	$-48.23 + 2.76B_{z,\mathrm{min}}$
$500 < V < 600$	$\mathrm{Dst_{min}} = -54.55 + 4.72B_{z,\mathrm{min}}$	$\mathrm{Dst_{min}} = -13.01 + 5.14B_{z,\mathrm{min}}$	$-47.66 + 3.70B_{z,\mathrm{min}}$
$600 < V < 750$	$\mathrm{Dst_{min}} = -66.72 + 7.53B_{z,\mathrm{min}}$	$\mathrm{Dst_{min}} = 75.96 + 10.43B_{z,\mathrm{min}}$	$-38.51 + 6.64B_{z,\mathrm{min}}$
$V > 750$	$\mathrm{Dst_{min}} = -147.07 + 2.84B_{z,\mathrm{min}}$	$\mathrm{Dst_{min}} = -32.14 + 4.54B_{z,\mathrm{min}}$	$-39.33 + 4.46B_{z,\mathrm{min}}$

[a]Range of averaged speed inside of the MC.

[b]Fitting function for the $\mathrm{Dst_{min}}$ linear estimation.

Table 8 Correlation coefficients between $\mathrm{Dst_{min}}$ and $B_{z,\mathrm{min}}$ for various $\langle V_{\mathrm{MC}}\rangle$ ranges for MCs without upstream shock wave.

Range of V [km s^{-1}][a]	# MCs	$\langle \mathrm{Dst_{min}}\rangle$[b]	CC[c]	Estimating Dst formula[d]
$V < 400$	48	−25	0.65	$\mathrm{Dst_{min}} = 8.75 + 5.71B_{z,\mathrm{min}}$
$400 < V < 500$	20	−38	0.74	$\mathrm{Dst_{min}} = -7.45 + 5.19B_{z,\mathrm{min}}$
$500 < V < 600$[e]	5	−41	0.99	$\mathrm{Dst_{min}} = 29.49 + 11.77B_{z,\mathrm{min}}$

[a]Range of averaged speed inside of the MC.

[b]Average of storm intensity.

[c]Correlation coefficients (CCs) of $\mathrm{Dst_{min}}$ versus $B_{z,\mathrm{min}}$ inside the MC.

[d]Fitting function for the $\mathrm{Dst_{min}}$ linear estimation.

[e]One MC has a solar wind speed faster than 600 km s^{-1}.

From the $\mathrm{Dst_{min}}$ estimating formulae listed in Tables 5 and 8, the estimated $\mathrm{Dst_{min}}$ are −78 nT for the MC on 4 March 1995, and −75.9 nT for the MC on 17 September, 2011. The errors of the predictions are 13.3 % and 8.4 % for the MC events that occurred in 1995 and

2011, respectively. It is interesting that the errors are larger than the best value by using Dst formulae that do not depend on velocity. Therefore, the Dst estimating-formulae listed in Table 2 are good for general use, at least on average. This may not hold for individual cases.

3. Summary

From *in situ* solar wind observations by the *Wind* spacecraft during 1995 – 2012, the main results of this study are as follows:

i) We identified 168 MCs and 197 MCLs, of which 94 MC_{shock} and 56 MCL_{shock} events had upstream shock waves.
ii) The average yearly occurrence rates for MCs, MCLs, MC_{shock}, and MCL_{shock} events are 9.3, 10.9, 5.2, and 3.1, respectively. The relative occurrence rate of MC_{shock} events (56 %) is about twice that for the MCL_{shock} events (28 %). The occurrence rate of automatically determined (Lepping, Wu, and Berdichevsky, 2005) MCs (and visually confirmed) is not related to the SSN, but the occurrence rate of MC_{shock} is well correlated with SSN during 1995 – 2012. The yearly occurrence rate of IP shocks is well correlated with SSN.
iii) The arrival time of an IP shock may be a good indicator for the initiation of a significant geomagnetic storm for space weather prediction because most MC-driven shock events cause strong geomagnetic storms (*e.g.*, $\langle Dst_{min} \rangle_{shock} = -102$ and -51 nT for MC_{shock} and MCL_{shock} events, respectively). An interplanetary shock can play an important role for the strength of a geomagnetic storm, as shown by the average intensity of geomagnetic storms associated with MC_{shock} which is ≈ 3.3 times higher than for the $MC_{no\text{-}shock}$.
iv) The averages of solar wind density, speed, thermal speed, and magnetic field for MC_{shock} events are higher than those for the $MC_{no\text{-}shock}$ events. The average solar wind speed is ≈ 25 % faster within MC_{shock} than within $MC_{no\text{-}shock}$. The average absolute value of $B_{z,min}$ is higher (> two times) within MC_{shock} than within $MC_{no\text{-}shock}$ events.
v) The average duration during 1995 – 2012 of an MC_{shock} event (19.8 h) is (≈ 11 %) longer than that of an $MC_{no\text{-}shock}$ event (17.6 h).
vi) Stronger MC storms follow a solar maximum, but MCLs do not show this trend.
vii) Choosing the correct Dst_{min} estimation-formula is very important for space weather predictions.
viii) Dynamic (or ram) pressure upstream of an MC/MCL event usually plays an important role in the intensity of a possible related geomagnetic storm.

The solar wind velocity plays an important role in affecting the intensity of a geomagnetic storm because the induced electric field at the magnetopause depends on V_{SW} through $B_z V_{SW}$, but also because a significant increase of velocity could cause a strong increase in the external ram pressure (ρV^2). Increased dynamic pressure, as caused by an ejecta-driven shock wave, would compress the Earth's front-side magnetopause toward Earth. This is due to the decreased size of the magnetosphere (according to $R_{MP} = R_o(B_o/B_{MP})^{1/3}$, where R_o is $R_{Earth} = 6378\ km$; B_o is the magnetic field on the Earth's surface), concomitant with the increased northern field of the front-side magnetosphere (B_{MP}), both caused by the increased external ram pressure on the magnetosphere resulting from the IP shock wave and density-enhanced sheath plasma. We speculate that the combination of a possible long-lasting southward field in fast-moving plasma in either the sheath or the MC/MCL structure and the ram pressure effect might cause enhanced storm intensities. Our statistical results seem to give relatively strong evidence of this expected effect.

Acknowledgements We are grateful to the *Wind* SWE and MFI teams, Kyoto University (Dst data), the World Data Center SILSO of the Royal Observatory of Belgium (sunspot number), NOAA/NGDC (which provided web access for sunspot number and Dst data sets), and the Harvard–Smithsonian Center for Astrophysics Interplanetary Shock Database (supported by NASA grant number NNX13AI75G) for the use of their data. Work of CCW is supported by the Chief of Naval Research.

References

Akasofu, S.-I.: 1981, Energy coupling between the solar wind and the magnetosphere. *Space Sci. Rev.* **28**, 121.

Burlaga, L.F.: 1988, *J. Geophys. Res.* **93**, 7217.

Burlaga, L.F.: 1995, *Interplanetary Magnetohydrodynamics*, Oxford University Press, New York, 89.

Burlaga, L.F., Sittler, E., Mariani, F., Schwenn, R.: 1981, *J. Geophys. Res.* **86**, 6673.

Echer, E., Gonzalez, W.D.: 2004, *Geophys. Res. Lett.* **31**, L09808.

Gopalswamy, N., Yashiro, S., Michalek, G., Xie, H., Lepping, R.P., Howard, R.A.: 2005, *Geophys. Res. Lett.* **32**, L12S09.

Kamide, Y., Yokoyama, N., Gonzalez, W., Tsurutani, B.T., Daglis, I.A., Brekke, A., Masuda, S.: 1998, *J. Geophys. Res.* **103**(A4), 6917. DOI.

Lepping, R.P., Burlaga, L.F., Jones, J.A.: 1990, Magnetic field structure of interplanetary magnetic clouds at 1 AU. *J. Geophys. Res.* **95**, 11957.

Lepping, R.P., Berdichevsky, D., Szabo, A., Lazarus, A.J., Thompson, B.J.: 2002, Upstream shocks and interplanetary magnetic cloud speed and expansion: Sun, WIND, and Earth observations. In: Lyu, L.-H. (ed.) *Space Weather Study using Multipoint Techniques*, *COSPAR Colloq. Ser.* **12**, Pergamon Press, Amsterdam, 87.

Lepping, R.P., Wu, C.C., Berdichevsky, D.B.: 2005, Automatic identification of magnetic clouds and cloud-like regions at 1 AU: Occurrence rate and other properties. *Ann. Geophys.* **23**, 2687.

Lepping, R.P., Berdichevsky, D.B., Wu, C.-C., Szabo, A., Narock, T., Mariani, F., Lazarus, A.J., Quivers, A.J.: 2006, A summary of WIND magnetic clouds for years 1995 – 2003: Model-fitted parameters, associated errors and classifications. *Ann. Geophys.* **24**, 215.

Lepping, R.P., Wu, C.C., Berdichevsky, D.B., Szabo, A.: 2012, Model parameter fittings and characterizations of Wind magnetic clouds for the period from early 2007 to fall 2012. AGU, Fall Meeting, SH41B-2109.

Lepping, R.P., Wu, C.C., Berdichevsky, D.B., Szabo, A.: 2015, Model parameter fittings and characterizations of Wind magnetic clouds for the period from early 2007 to 2012. *Solar Phys.* **290**(8), 2265. DOI.

Shue, J.-H., Song, P., Russell, C., Steinberg, J.T., Chao, J.K., Zastenker, G., *et al.*: 1998, Magnetopause location under extreme solar wind conditions. *J. Geophys. Res.* **103**, 17691.

Tsurutani, B.T., Smith, E.J., Gonzalez, W.D., Tang, F., Akasofu, S.I.: 1997, Origin of interplanetary southward magnetic fields responsible for major magnetic storms near solar maximum (1978 – 1979). *J. Geophys. Res.* **93**, 8517.

Tsurutani, B.T., Gonzalez, W.D.: 1997, The interplanetary causes of magnetic storms: A review. In: Tsurutani, B.T., Gonzalez, W.D., Kamide, Y. (eds.) *AGU Geophys. Monogr.* **98**, 77.

Wang, Y.M., Ye, P.Z., Wang, S., Xue, X.H.: 2003, An interplanetary cause of large geomagnetic storms: Fast forward shock overtaking preceding magnetic cloud. *Geophys. Res. Lett.* **30**, 1700.

Wu, C.-C., Lepping, R.P.: 2002a, Effects of magnetic clouds on the occurrence of geomagnetic storms: The first 4 years of Wind. *J. Geophys. Res.* **107**, 1314.

Wu, C.-C., Lepping, R.P.: 2002b, Effect of solar wind velocity on magnetic cloud-associated magnetic storm intensity. *J. Geophys. Res.* **107**, 1346.

Wu, C.-C., Lepping, R.P.: 2005, Relationships for predicting magnetic cloud-related geomagnetic storm intensity. *J. Atmos. Solar-Terr. Phys.* **67**, 283.

Wu, C.-C., Lepping, R.P.: 2007, Comparison of the characteristics of magnetic clouds and magnetic cloud-Like structures for the event of 1995 – 2003. *Solar Phys.* **242**, 159.

Wu, C.-C., Lepping, R.P.: 2008, Geomagnetic activity associated with magnetic clouds, magnetic cloud-like structures and interplanetary shocks for the period 1995 – 2003. *Adv. Space Res.* **41**, 335.

Wu, C.-C., Lepping, R.P., Gopalswamy, N.: 2003, Variations of magnetic clouds and CMEs with solar activity cycle. In: Wilson, A. (ed.) *Proc. International Solar Cycle Studies Symposium, Solar Variability as an Input to the Earth's Environment*, *ESA SP-535*, 429.

Wu, C.-C., Lepping, R.P., Gopalswamy, N.: 2006, Relationships among magnetic clouds, CMES, and geomagnetic storms. *Solar Phys.* **239**, 449.

Wu, C.-C., Lepping, R.P.: 2011, *Solar Phys.* **269**(1), 141. DOI.

Wu, C.-C., Lepping, R.P.: 2015, *Solar Phys.* **290**(4), 1243. DOI.